Journal of the Iranian Chemical Society (2022) 19:3697–3709
https://doi.org/10.1007/s13738-022-02564-1

ORIGINAL PAPER

Cu(II) immobilized on guanidine functionalized Fe_3O_4 magnetic substrate as a heterogeneous catalyst for selective reduction of nitroarenes

Guddappa Halligudra[1] · Chitrabanu Chikkanayakanahalli Paramesh[1] · Manjunath Shetty[1] · Harsha Kachigere Bhadraiah[2] · Vinaya Kambappa[3] · Ananda Kumar Channapillekoppalu Siddegowda[1] · Dinesh Rangappa[1] · Rangappa Kanchugarakoppal Subbegowda[4] · Prasanna Doddakunche Shivaramu[1]

Received: 30 July 2021 / Accepted: 8 April 2022 / Published online: 3 May 2022

Abstract
In the present work, copper (II) immobilized on guanidine functionalized Fe_3O_4 nanoparticles (Fe_3O_4@Guanidine–Cu^{II}) are developed as a heterogeneous catalyst. Fe_3O_4@Guanidine–Cu^{II} is well-characterized by adopting FT-IR, XRD, SEM, TEM, EDX, SEM-elemental mapping, TG–DTA, XPS, ICP-OES, and VSM analysis. Fe_3O_4@Guanidine–Cu^{II} is employed for the selective reduction of nitro group on electronically diversified nitroarenes involving $NaBH_4$ to serve as a hydrogen source in ethanol medium. Anilines resulted from the reduction of nitroarenes are of excellent yields with high TON and TOF numbers, indicating the efficiency of the prepared catalyst. Also, the catalyst has been recovered with effective yield over the time of the reaction, and the recovered catalyst was used up to eight cycles for the reaction without any significant change in the catalytic activity. This notable feature of the prepared catalytic system makes it highly promising, not only for an industrial but also from an environmental point of view.

Keywords Catalysis · Heterogeneous magnetic catalyst · Nitroarenes reduction · Cu(II)-based catalyst

Introduction

Nitroarenes are one of the major classes of organic pollutants released by various industries into the aqueous systems, which are hazardous primarily to the environment and further toxic to human beings, animals and plants. The US Environmental Protection Agency announced that nitrobenzene, 4-nitrophenol, 2-nitroaniline and similar nitro group-bearing molecules are highly noxious pollutants as it easily gets dissolved into water and causes adverse conditions to the aquatic organisms [1, 2]. These nitroaromatic compounds are being used as industrial chemicals as it contributes a crucial function in the preparation of medicines, dyes, pigments, plastics, insecticides, bactericides, explosives, along with industrial solvents [3, 4]. This is one of the most important areas to be addressed by the researchers to convert these toxic nitroarenes to non-toxic and valuable intermediates and products. These are known to be readily available, starting materials in the process of organic synthesis. Nitroarenes can be converted to corresponding less toxic and readily biodegradable amines through the reduction by various methods such as wet-air oxidation [5], photodegradation method [6–8], electrochemical reduction [9], and also catalytic reduction [10] have been developed by the researchers around the world. The catalytic reduction method is being evolved as the most promising and one among the numerous existing reduction methods [11].

✉ Dinesh Rangappa
dineshrangappa@gmail.com

✉ Rangappa Kanchugarakoppal Subbegowda
rangappaks@yahoo.com

✉ Prasanna Doddakunche Shivaramu
prasuds@gmail.com

[1] Department of Applied Sciences, Centre for Postgraduate Studies, Visvesvaraya Technological University, Muddenahalli, Bengaluru Region, Chikkaballapur District 562 101, India

[2] Center for Material Science, University of Mysore, Vijnana Bhavana, Manasagangotri, Mysuru 570006, India

[3] Department of Chemistry, Government First Grade College, Kadur 577548, India

[4] Institution of Excellence, University of Mysore, Vijnana Bhavana, Manasagangotri, Mysuru 570006, India

Most of these catalytic reduction methods involve the presence of one or more metal-based catalysts, namely Ru/SiO_2[12], Pd [13], Pt [13], V [13], Pt/Ni [14], Pt/Pd [15], and coinage metal nanoparticles (Au/Ag) [16]. But they have significantly increased total costs because of high-cost precious metals and their limited availability. This has also led scientists to explore affordable and eco-friendly replacements. Copper (II) acetylacetonate-based catalyst has been reported to be an immensely particular homogeneous catalyst used to reduce nitro compounds. From the fact that Cu is ample and convenient compared to other metals previously described, the application of copper-based catalysts turns out to be a cost-effective approach [17]. Homogeneous reductions of nitroarenes using various copper-based catalysts are already reported by researchers [18]. Even though homogeneous copper-based catalysts are very effective and selective in their action, difficulty in removing and/or recovery and reusability of the catalysts hinders the process of homogeneous catalysis overcome this difficulty; researchers have come up with copper-based heterogeneous catalysts [19, 20]. Solid-phase organocopper complexes with high activity and selectivity provide several practical advantages: ease of obtaining the catalyst by the desired product along with reduction of the overall cost in the processes. Along these lines, immobilization methods accommodating copper on heterogeneous solid beds have been extensively studied [21]. However, these studies seem not to support the fast segregation with the entire uptake of catalyst. Magnetic nanoparticle substrate supported catalyst makes the separation of the catalyst effortless and makes the complete revival of catalyst possible arising out of the reaction mixture. This prevents aggregation of nanoparticles during regeneration and increases the catalyst durability [22]. This type of magnetic substrate-supported catalyst separation needs no use of filtration and centrifugation. Therefore, the magnetic composites can be segregated appropriately and collected by employing a required magnetic field within the reaction mixture [23, 24].

Immobilization of ligand to the substrate's surface possess a significant impact on the tuning of catalytic potential of materials and their stability at ambient temperature in air or aqueous medium [25]. The use of adequately supported ligands for heterogenized substrates provides a substantial and renewable catalytic method in addition to minimal leaching and avoids accumulation problems [26]. In this context, nitrogenous ligands have received more attention as they possess intensified thermal stability, low cost, high productivity, and easy synthesizing methods [27]. Various such metal complexes containing N-ligand and their derivatives like imidazole [28], Schiff bases [29], pyridine [30], NNN-pincer ligands [31], N-containing dendrimers [32], DABCO [33] and thiols [34], have been used as active catalysts in synthetic organic chemistry. Among these, guanidine is an essential class of naturally occurring compounds, frequently used in natural science, and is substantially used as catalysts. Specifically, guanidine is a suitable N-donor ligand due to its ability to shift a positive charge to the guanidine moiety, a behavior that results in highly basic and highly nucleophilic compounds with improved ability to coordinate with metal ions. As a result, guanidine-type ligands have been distinctively utilized to develop highly active homogeneous/heterogeneous catalysis with transition metals, which can catalyze various organic reactions [35–37].

Although most of the reported catalysts and protocols are helpful in the reduction of nitroarenes, they usually suffer from a long reaction time, low yield, selectivity, and the use of expensive and excess reagents. Thus, this alternative will be active, simple, environmentally friendly, and the use of reusable catalysts could be of best interest.

Within the framework of our present investigation and based on the above-mentioned criteria for evaluating novel catalysts systems and methods for various reactions and applications, we have synthesized novel Cu^{II}-based guanidine conjugated iron oxide nanoparticles that are immensely competent, magnetically separable, and could be used several times. The catalytic activity of Fe_3O_4@Guanidine-Cu^{II} was subsequently investigated toward the selective reduction of nitroarenes in ethanol media at ambient conditions.

Experimental

Materials and methods

All the employed chemicals and solvents are of Merck and Sigma-Aldrich. They were used during synthesis without any further purification. The purity of the products and the advancement of organic reactions were screened with Thin-layer chromatography (TLC) on TLC Silica gel 60 F_{254} Plates. The prepared catalyst materials were examined for their crystal structure using a Rigaku *x*-ray diffractometer. The catalyst's particle size along with surface morphology was analyzed by SEM (HITACHI SU15010) and HR-TEM (Jeol/JEM 2100). The Functional group analysis was accomplished using FT-IR (Perkin Elmer Spectrum Two). The uniform distribution of elements on the catalyst surface was analyzed by SEM-elemental mapping from ZEISS EVO 18. The differential thermal analysis (DTA), as well as thermogravimetric analysis (TGA), were conducted by employing Perkin Elmer STA 8000. The catalyst's elemental analysis and oxidation states were effectuated by x-ray Photoelectron Spectroscopy (XPS) from ULVAC-PHI Japan. The metal ion concentration is performed by using inductively coupled plasma optical emission spectroscopy (ICP-OES) from Perkin Elmer Optima 5300DV. A vibrating sample magnetometer (VSM) of Lakeshore VSM7410 make was used to

examine the magnetic properties of the catalyst maintained at ambient conditions.

Preparation of Fe_3O_4 nanoparticles

Fe_3O_4 nanoparticles were obtained following the previously reported method [38]. The regular synthesis procedure includes dissolving ferric chloride hexahydrate (2.16 g) in ethylene glycol (EG) (40 ml) and stirred for 30 min to get the transparent solution. Then it was followed by the addition of sodium acetate (3.60 g) along with sodium dodecyl sulfate (0.50 g) to this mixture and continuously stirred for about 30 min. Then the resulting solution is placed in a 50 ml Teflon-based stainless-steel autoclave, heated for 12 h at a temperature of 200 °C. By the end of the process, Fe_3O_4 nanoparticles were gathered by utilizing an external magnet and then washed several times using distilled water (DI-H_2O) (5 × 5 ml) and ethanol (EtOH) (2 × 5 ml). The obtained product was dried using a sealed vacuum oven maintained at 60 °C for 6 h and the final product is represented as Fe_3O_4.

Preparation of guanidine conjugated Fe_3O_4 nanoparticles

The synthesized Fe_3O_4 nanoparticles (1.00 g) were dispersed in ethanol and then sonicated for 10 min. Later we mixed 1-Bromo-3-chloropropane (4.31 mmol) in them and agitated them for 6 h in ambient conditions. By the end of the process, the final product is separated using an external magnet in addition to washing by EtOH (5 × 5 ml) and drying. The dried powder (0.254 g) was later mixed in dry toluene followed by sonication for 10 min. Then continued by addition of guanidine hydrochloride (0.109 g, 1.1 mmol) along with sodium bicarbonate (0.193 g, 2.3 mmol) to these stirring chemicals and refluxed for 12 h. After finishing this process, we segregated the solid using an external magnet and then rinsed utilizing dichloromethane (CH_2Cl_2) (3 × 5 ml), EtOH (2 × 5 ml). The obtained product was dried at 60 °C for 6 h.

Immobilization of Cu^{II} on guanidine conjugated Fe_3O_4 nanoparticles

The synthesized Fe_3O_4@Guanidine (0.35 g) was sonicated in methanol for 30 min. It was followed by the addition of copper (II) acetate (0.288 g, 1.4 mmol) and the mixture was refluxed for 6 h. This formed complex was then collected with the help of an external magnet, and continued by washing with DI-H_2O (5 × 5 ml), EtOH (3 × 5 ml), along with drying in 60 °C for 6 h in the oven to get Fe_3O_4@Guanidine-Cu^{II}.

The general method for selective reduction of nitroarenes

This procedure includes the addition of Fe_3O_4@Guanidine-Cu^{II} (0.6 mol %) to nitro compound (1 mmol) and $NaBH_4$ (3 mmol) in ethanol (2 ml) within ambient conditions and agitated for an appropriate period (Table 1). With the help of TLC, the advancement in reduction is regulated. Later, the catalyst particles were separated using an external magnet, in addition to washing the mixture with ethyl acetate (EtOAc) (2 × 5 ml) and H_2O (3 × 5 ml). Then anhydrous Na_2SO_4 was used to dehydrate the organic layer and thus the solvent was evaporated to recover the crude resultants with reduced pressure. The final step was performed by eluting the product with n-hexane: ethyl acetate (4:1) solution in column chromatography packed with silica gel.

Results and discussion

Preparation and characterization of Fe_3O_4@guanidine-Cu^{II}

In recent years, the progress relating to novel heterogeneous catalysts by organic reaction has become an important research area in chemical sciences. Herein, we report a unique, environmentally safe and recyclable catalyst which is copper-based guanidine conjugated heterogeneous magnetic-based for selective reduction of nitroarenes at room temperature. Scheme 1 indicates the pathway; we have followed to prepare Fe_3O_4@Guanidine-Cu^{II}. For catalyst preparation, the core–shell Fe_3O_4 nanoparticles were conjugated using 1-Bromo-3-chloropropane by the nucleophilic substitution reaction along with guanidine ligand. Later we combined Fe_3O_4@Guanidine with copper acetate solution and refluxed for 6 h to incorporate copper ions.

We performed FT-IR spectral analysis for reaffirming the Fe_3O_4, Conjugation of guanidine, and copper incorporation onto guanidine. As observed in Fig. 1a, peaks at 3403 and 1620 cm^{-1} corresponds to Fe_3O_4 ascribed to attached O–H groups and adsorbed H_2O molecules [39]. The presence of Fe_3O_4 nanoparticles was affirmed due to peaks emerging at 550 cm^{-1} and was ascribed for the Fe–O stretching oscillation of Fe_3O_4 (Fig. 1) [40]. Vibration bands at 1652 cm^{-1} (C=N), 1427 cm^{-1} (C–N), and 830 cm^{-1} (–NH_2) in the FTIR spectra Fe_3O_4@Guanidine confirmed conjugation of guanidine molecule onto magnetic nanoparticles [36]. In FTIR spectra of Fe_3O_4@Guanidine-Cu^{II}, as a matter of curiosity upon the metalation of copper ions, absorption of C=N bond at 1652 cm^{-1}in the

Table 1 Optimization of the reaction parameters for reduction of nitrobenzene to aniline

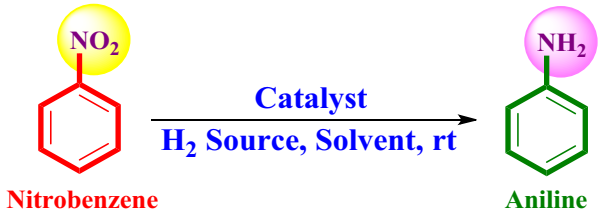

Entry[a]	Catalyst (mol%)	Molar ratio of NB: H_2 source (mmol)	Hydrogen Source	Solvent	Time (min)	Isolated Yield (%)
1	Without catalyst	1:3	$NaBH_4$	EtOH	24 h	No reaction
2	0.2	1:3	$NaBH_4$	EtOH	50	67
3	0.4	1:3	$NaBH_4$	EtOH	45	83
4	0.6	1:3	$NaBH_4$	EtOH	30	99
5	0.8	1:3	$NaBH_4$	EtOH	30	99
6	0.6	1:1	$NaBH_4$	EtOH	60	81
7	0.6	1:2	$NaBH_4$	EtOH	50	87
8	0.6	1:4	$NaBH_4$	EtOH	25	90
9	0.6	1:3	$H_2N–NH_2$	EtOH	40	80
10	0.6	1:3	$NaBH_4$	H_2O	50	82
11	0.6	1:3	$NaBH_4$	EtOH: H_2O (1:1)	60	89
12	0.6	1:3	$NaBH_4$	Methanol	120	80
13 [b]	0.6	1:3	$NaBH_4$	EtOH	110	50
14 [c]	0.6	1:3	$NaBH_4$	EtOH	60	71

[a]Optimized reaction conditions: Nitrobenzene (1 mmol), $NaBH_4$ (3 mmol), and Fe_3O_4@Guanidine-Cu^{II} (0.6 mol%) catalyst were stirred at room temperature for 30 min. [b]CuO nanoparticles, [c]Fe_3O_4@SiO_2@CuO nanoparticles

Scheme. 1 Schematic diagram showing the synthesis of Fe_3O_4@Guanidine-Cu^{II}

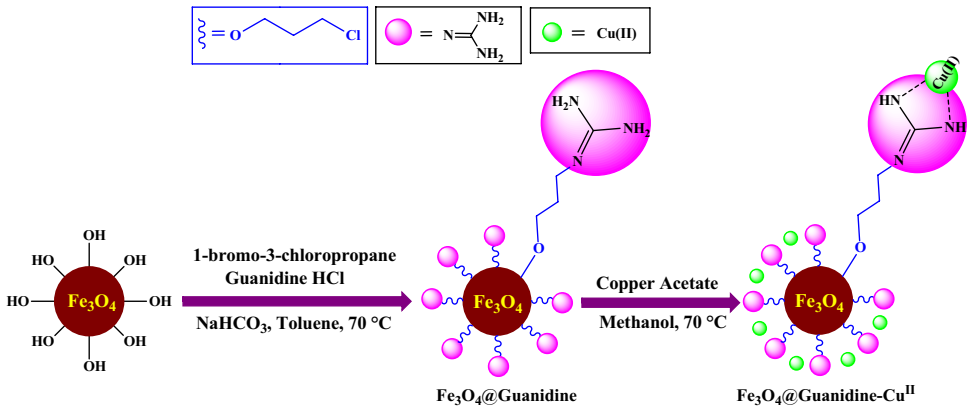

spectra of Fe_3O_4@Guanidine were shifted to 1545 cm^{-1}. These results confirmed the coordination of the metal with a ligand molecule [38, 41].

Figure 2 represents the Fe_3O_4, Fe_3O_4@Guanidine, and Fe_3O_4@Guanidine-Cu^{II} patterns obtained by the x-ray diffractometer. The presence of Fe_3O_4 nanoparticles are recognized using diffraction peaks positioned at $2\theta = 18.3°$, 30.1°, 35.4°, 43.1°, 53.4°, 56.9°, and 62.5°. It indicated that Fe_3O_4 nanoparticles fairly comprises the face-centered cubic inverse spinel arrangement of magnetite (JCPDS No.19–0629) [42]. The XRD image of the Fe_3O_4@Guanidine-Cu^{II} complex indicates the magnetite crystalline arrangement, as well as the features of the Fe_3O_4 center, is maintained following the conjugation. Hence the obtained findings validate that guanidine ligands have been effectively conjugated on top of Fe_3O_4 nanoparticles [43].

The evaluated particle size along with morphology is recorded by the SEM and TEM images, as shown in Fig. 3. As noticed in Fig. 3(a & b), Fe_3O_4 particles are spherical with nanometer-sized particles. Aggregations of Fe_3O_4

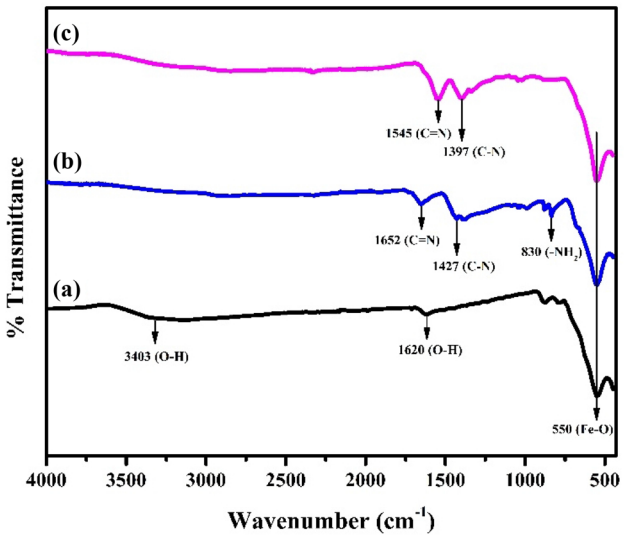

Fig. 1 FTIR spectra of **a** Fe_3O_4 nanoparticles showing the transmittance peak at 550 cm^{-1} correspond to Fe–O bond, **b** Fe_3O_4@Guanidine showing absorption peak at 1652 cm^{-1}, 1427 cm^{-1}, and 830 cm^{-1} correspond to (C=N), (C–N), ($–NH_2$) bonds and **c** Fe_3O_4@Guanidine-Cu^{II} showing absorption peak at 1545 cm^{-1} (shifted peak) corresponding to (C=N), confirms coordination of metal with a ligand molecule

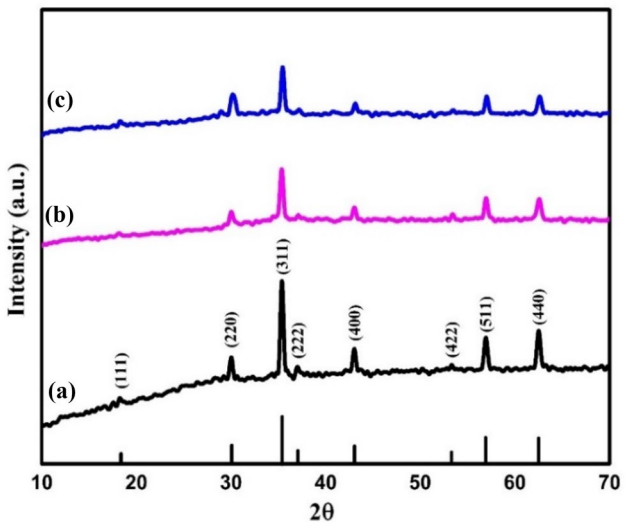

Fig. 2 XRD patterns of **a** Fe_3O_4 **b** Fe_3O_4@Guanidine, **c** Fe_3O_4@Guanidine-Cu^{II} showing the peaks at 18.3° (111), 30.1° (220), 35.4° (311), 43.1° (400), 53.4° (422), 56.9° (511), and 62.5° (440) corresponding to FCC inverse spinel structure of Fe_3O_4

nanoparticles are also seen due to the magnetostatic interaction of the particles. The TEM images of Fe_3O_4@Guanidine-Cu^{II} in Fig. 3(c, d, e & f) confirm the layer on the iron oxide nanoparticles' core–shell structure and immobilized guanidine layer on the surface. As can be seen in Fig. 3(e & f), Cu nanoparticles are relatively uniformly dispersed on the magnetic guanidine surface, and their average particle size is determined in the range of 30–60 nm. We have resolved the elemental composition of nanocatalyst by EDX instrumentation and Fig. 3g describes that Fe_3O_4@Guanidine-Cu^{II} catalyst contains elements C, N, Fe, O, and Cu, which is in accordance with SEM-elemental mapping results (Fig. 4). The elemental mapping revealed no other elements other than C, N, Fe, O, and Cu, demonstrating that the preparation technique is reliable. Moreover, the mapping results showed the uniform grafting of the guanidine ligand on the Fe_3O_4 surface.

TGA analysis of Fe_3O_4@Guanidine-Cu^{II} (Fig. 5) showed a weight loss of 1% below 180 °C, which is because of decomposition of physically chemisorbed solvents along with surface hydroxyl members [44]. A weight loss of about 2.3% had occurred between 260 °C to 350 °C due to the metal–organic structural decomposition. The organic functional group has been known to decompose over 200 °C. The four consecutive weight losses around 9.72% at 200 to 650 °C, which are by the means of decomposition of organic ligands conjugated above the magnetic nanoparticles. Thus, this analysis revealed that the guanidine molecule was successfully conjugated with magnetic nanoparticles [38, 45]. The DTA diagram (Blue line) showed that Fe_3O_4@Guanidine-Cu^{II} was degraded in two steps below 100 °C and 325 °C, followed by an endothermic process related to the decomposition of adsorbed water/solvent and organic ligand from the surface of the catalyst. The peak in the DTA curve showed that the fastest loss of the organic ligand occurred at 325 °C. Therefore, the Fe_3O_4@Guanidine-Cu^{II} were stable below about 200 °C.

XPS studies were performed to investigate the chemical composition and oxidation state of synthesized Fe_3O_4@Guanidine-Cu^{II} nanocatalyst (Fig. 6). Figure 6a represents the overall XPS patterns of Fe_3O_4@Guanidine-Cu^{II}, which contains the peaks corresponding to O, C, N, Fe, and Cu. Figure 6b indicates the XPS pattern relating to C 1s that might get de-convoluted to two major peaks at 285.77 eV as well as at 288.82 eV, which correspond to $C_{sp}{}^2$-N and $C_{sp}{}^3$-N bonds. Figure 6c shows XPS spectra relating to N 1s; it reveals that the major peak at 401 eV is associated with C–N–C, along with two more peaks at 399.9 eV and 399 eV which were associated with the $C_{sp}{}^2$-N and $C_{sp}{}^3$-N bond. Figure 6d, reveals the spectra relating to Fe 2p with deconvolution of Fe ($2p_{1/2}$) ($2p_{3/2}$) spectrum showing major peaks at 723.9 eV, 711.87 eV (Fe^{3+}) and 722.16 eV, 710.3 eV (Fe^{2+}), which affirms that the position of the Fe ($2p_{1/2}$) ($2p_{3/2}$) peaks corresponds to Fe_3O_4[38, 46]. In Fig. 6e, the Cu $2p_{3/2}$ peaks could be de-convoluted into two main peaks at 934.86 eV and 933.21 eV that matched appropriately with Cu^{2+} octahedral as well Cu^{2+} tetrahedral types. During synthesis in ethanol medium, Cu was reduced to Cu (0), where ethanol media acts as a reducing

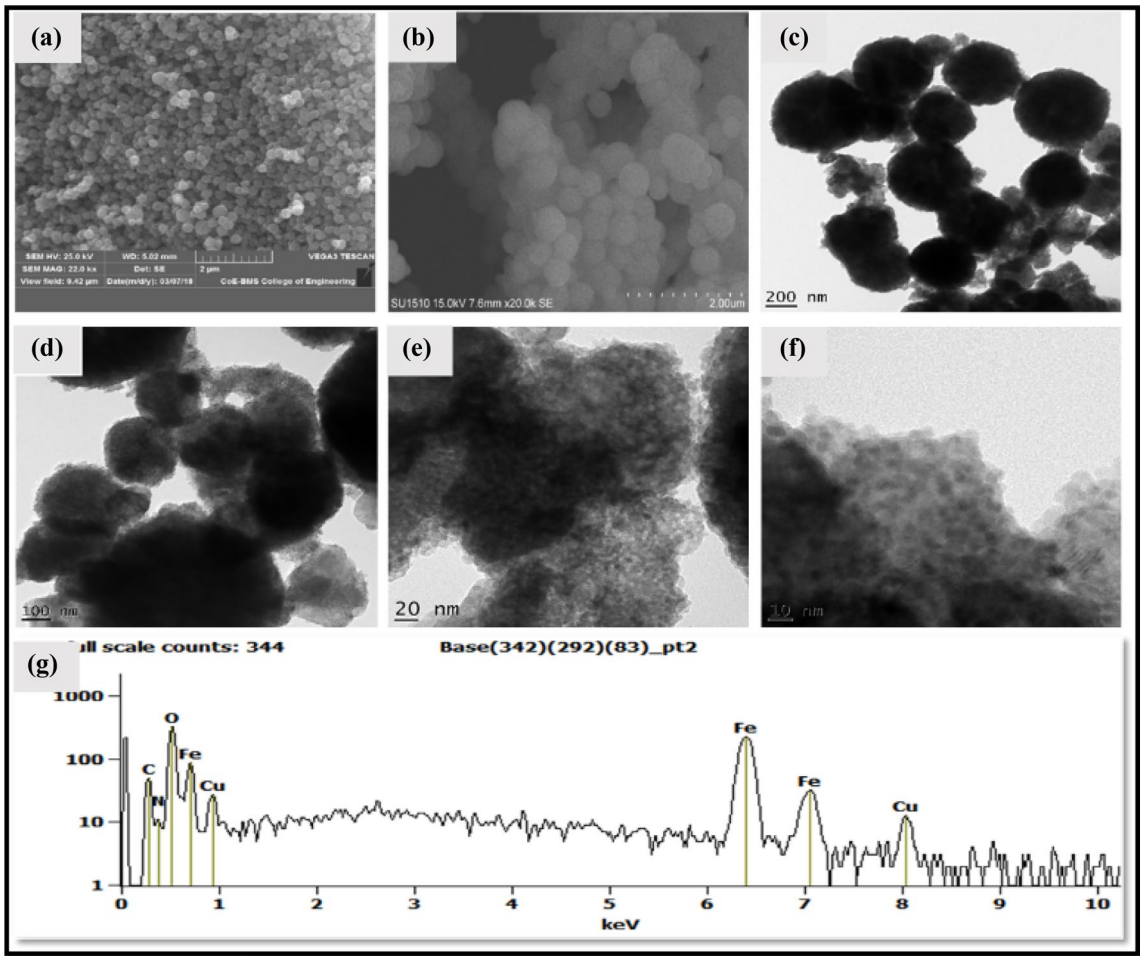

Fig. 3 **a** FE-SEM image of Fe_3O_4 confirms the spherical structure of Fe_3O_4 **b** SEM image of Fe_3O_4@Guanidine-Cu^{II} confirms the spherical structure of Fe_3O_4@Guanidine-Cu^{II}, (**c**, **d**, **e** & **f**) TEM images of Fe_3O_4@Guanidine-Cu^{II} confirms layer on core–shell arrangement of the iron oxide nanoparticles and immobilized guanidine layer on the surface, and **g** EDX spectra of Fe_3O_4@Guanidine-Cu^{II} confirming the presence of C, O, Fe, Cu, N

agent[25], and then reduced Cu with 0, 1 oxidation states observed at 933.21 eV. This result also confirms the presence of Cu^{2+} and Cu^{+}/Cu[47, 48].

As mentioned, the Cu^{II} content of Fe_3O_4@Guanidine-Cu^{II} is assessed using ICP-OES. The ICP-OES determination indicated 0.834 mmoles of Cu were held tight to 1 g Fe_3O_4@Guanidine-Cu^{II}.

The magnetic features relating to Fe_3O_4 and Fe_3O_4-Guanidine-Cu^{II} are studied using VSM in ambient conditions and are displayed in Fig. 7. The saturation magnetization (*Ms*) value of the Fe_3O_4@Guanidine-Cu^{II} (1.144 emu) is less than that of Fe_3O_4 (1.2238 emu) nanoparticles due to the organic layer and copper material on top of Fe_3O_4 nanoparticles. These weak hysteresis loops are demonstrated by the magnetization evidence at room temperature, indicating that ferromagnetic behavior exists in all Fe_3O_4 core and Fe_3O_4@Guanidine-Cu^{II} samples. Consequently, the developed magnetic nanoparticles possess typical ferromagnetic performance that could be proficiently gathered to a single place using a small magnet [38].

Catalytic selective reduction of nitroarenes

Following the effective synthesis and characterization of Fe_3O_4@Guanidine-Cu^{II}, exploring the activity of the heterogeneous catalyst was investigated initially to reduce nitroarenes. At the preliminary step, we enhanced the reaction conditions by changing solvent, hydrogen source, and catalyst quantity considering the prototype reaction of nitrobenzene (1 mmol) as shown in Table 1. We performed the blank trials without involving the catalyst in ethanol at room temperature using 1:3 molar ratios, yielding only a minute quantity of product despite extended duration. In the next step, to examine the solvents' influence, including C_2H_5OH, CH_3OH, H_2O, and C_2H_5OH/H_2O (1:1), are

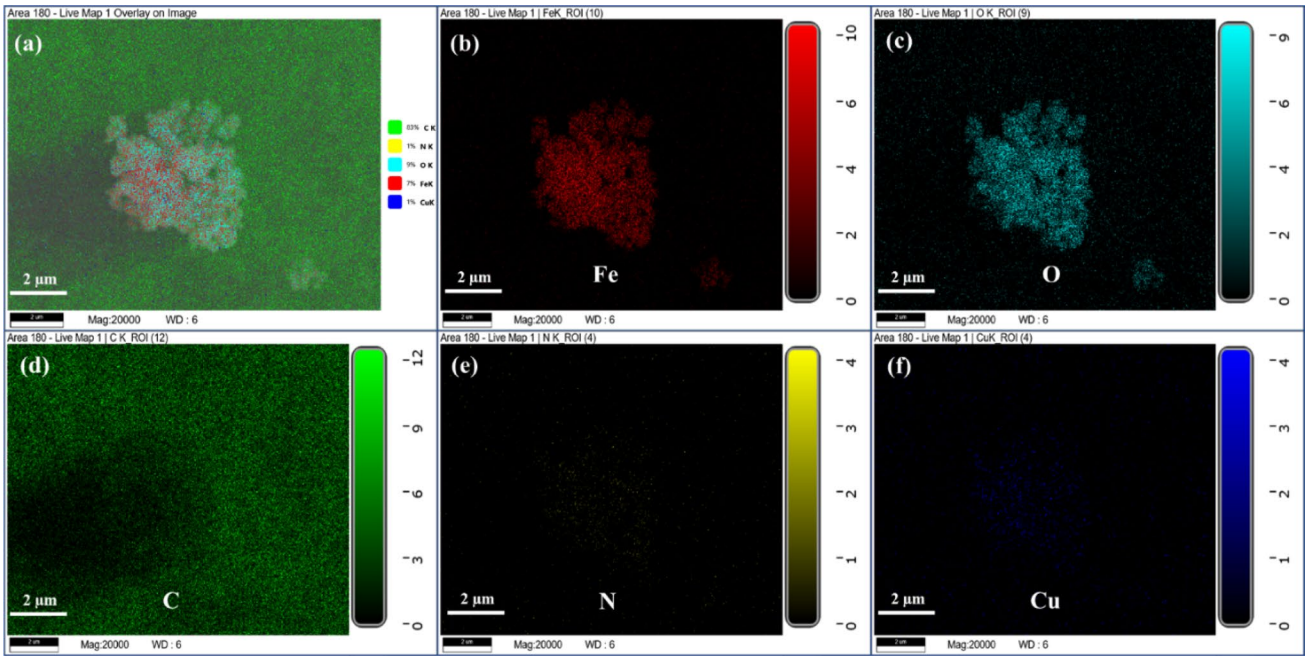

Fig. 4 Elemental mapping of Fe_3O_4@Guanidine-Cu^{II} **a** overall, **b** Fe, **c** O, **d** C, **e** N, **f** Cu confirming the presence of C, O, Fe, Cu, N

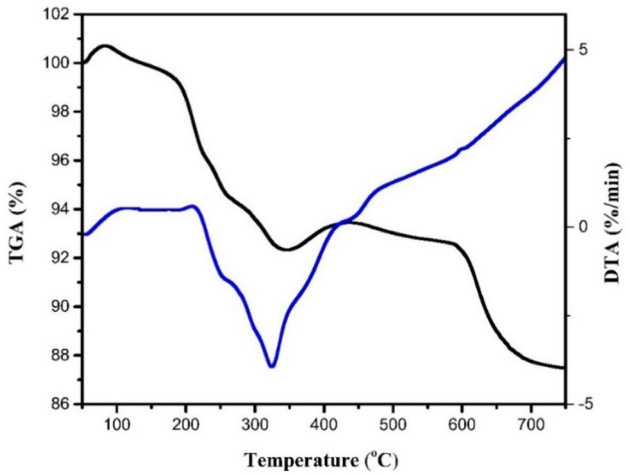

Fig. 5 TG–DTA diagram of Fe_3O_4@Guanidine-Cu^{II} showing the weight loss of around 9.72% at 200 to 650 °C, indicating the decomposition of organic ligands conjugated on the surface of magnetic nanoparticles

examined under the existence of 0.6 mol% of the catalyst with identical reaction parameters. These experiments led us to found that C_2H_5OH is superior among the used solvents (Table 1). A series of available hydrogen sources, such as $NaBH_4$, NH_2-NH_2, CH_3COOH, and CH_2O_2, were screened to determine the effect of hydrogen sources on reaction rate. Hydrogen sources such as $NaBH_4$ and NH_2-NH_2 were found to be more effective compared to CH_3COOH and CH_2O_2. This could be because of the high solubility of hydrogen sources in the ethanol media. Thus, $NaBH_4$ was considered for further reactions as an excellent choice in terms of financial and reaction progress viewpoints (Table 1). During the enhancement work, the immediate impact of employing a varied molar ratio of nitrobenzene/$NaBH_4$ was explored. As per the observations made, a decrease in reaction rate was noticed by the decreasing amount of $NaBH_4$ to 2 mmol. There was no further development noticed by increasing the amount of $NaBH_4$ to 4 mmol (Table 1). With an effort to search for more optimal conditions, the catalyst amount's effect was further evaluated. Later, different amounts of supported copper catalysts were examined in the reduction reactions of nitrobenzene. By illustrating in Table 1, the use of 0.6 mol% of the catalyst in the nitroarene reduction reaction gave the best results. When the conditions were kept constant, the effect of using various catalysts was further investigated. Finally, using a 1:3 mmol ratio of nitrobenzene/$NaBH_4$ in ambient conditions by the existence of 0.6 mol % of Fe_3O_4@Guanidine-Cu^{II} in ethanol media was selected as the best-optimized condition to carry out further reactions (Table 1).

The reduction reaction scope was extended to various nitroarenes with such optimized conditions and high TON and TOF, as shown in Table 2. In all instances, the reduction reaction was finished by 60 min resulting in excellent yields (57–99%) (Table 2). Nitroarenes including o-Chloro, m-Chloro, 3-Bromo, 4-Bromo, and p-Fluoro (Table 2) are completely reduced to corresponding amines devoid of any dehalogenation. Electron-donating entities (such as –OCH_3

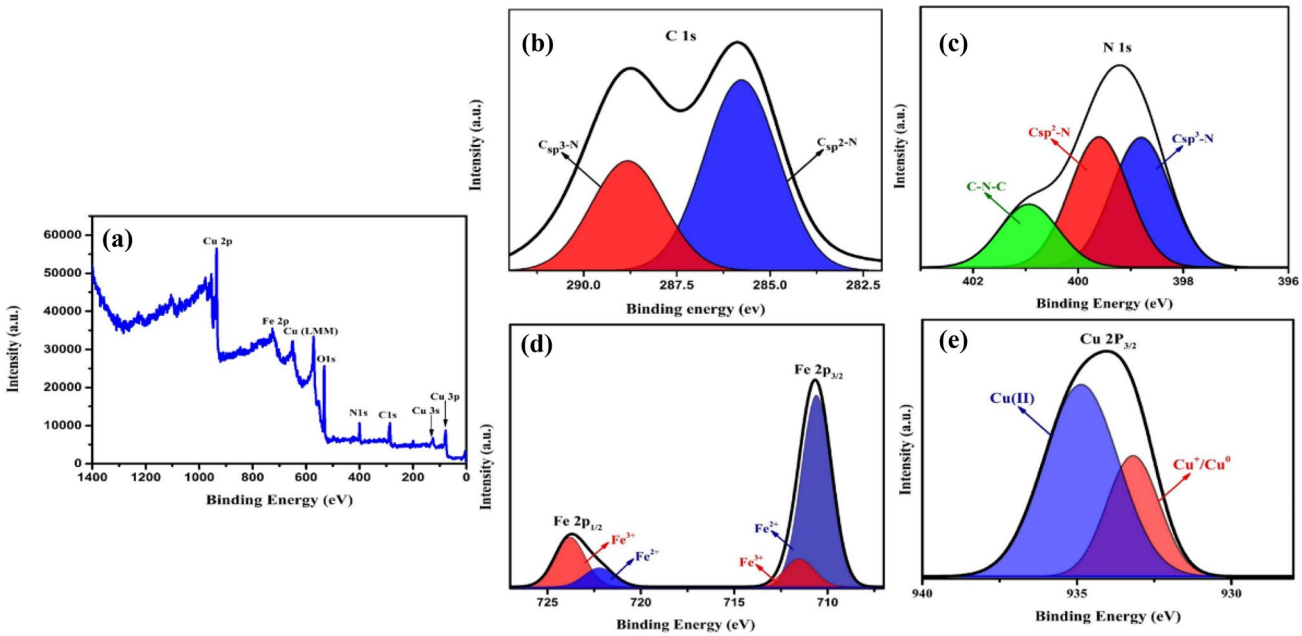

Fig. 6 **a** Overall XPS patterns of Fe_3O_4@Guanidine-Cu^{II} confirming the presence of O, C, N, Fe, Cu **b** C 1s showing peaks at 285.77 eV, 288.82 eV corresponding to Csp^2-N, Csp^3-N bond **c** N 1s showing the peaks at 401 eV, 399.9 eV and 399 eV corresponding to C–N–C, Csp^2-N and Csp^3-N bond **d** Fe 2p showing peaks at major peak at 723.9 eV, 711.87 eV (Fe^{3+}) and 722.16 eV, 710.3 eV (Fe^{2+}) corresponding to Fe_3O_4 **e** Cu 2P showing the peaks at 934.86 eV, 933.21 eV corresponding to Cu^{2+}

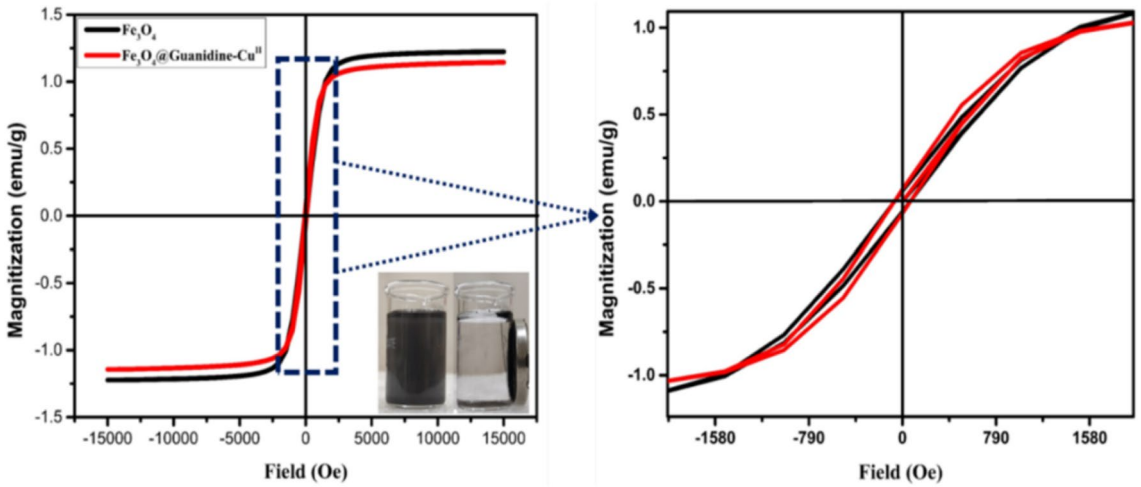

Fig. 7 Magnetization curves of Fe_3O_4 and Fe_3O_4-Guanidine-Cu^{II} showing the weak hysteresis loop indicating the ferromagnetic behavior of the prepared material

and $–CH_3$) and electron-withdrawing entities (such as –C=OR along with –COOH) are preferably altered to similar amines resulting in satisfactory returns. Reduction of o-nitrophenol, m-nitrophenol, p-nitrophenol, and 2-chloro-p-nitrophenol with sodium borohydride results in the corresponding amino compound within 20–40 min without disturbing the –OH group. After completing the reaction, pure products were achieved by simple work-up, including magnetic separation and column chromatography. The formed products were confirmed by recording ^{1}H NMR spectra, checking their mp/bp, and comparing them with the data available in the literature.

Comparative study

Finally, the catalytic efficiency of Fe_3O_4@Guanidine-Cu^{II} was compared with the previously mentioned catalysts for the reduction of nitroarenes are described in Table 3.

Table 2 Reaction time, isolated yield, the melting point of the obtained products in the reduction of electronically diversified nitroarenes[a]

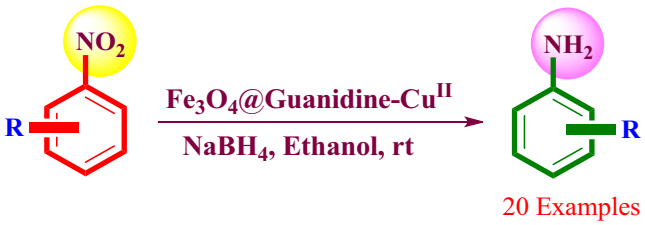

Entry[a]	Product	Time (min)	Isolated Yield (%)	TON	TOF (h^{-1})	mp(°C)/ bp(°C)		[ref]
						Obtained	Reported	
1	Aniline	30	99	165	330	184[b]	184.1[b]	[50]
2	2-aminophenol	20	92	154	462	170–173	170–175	[51]
3	3-aminophenol	20	89	149	447	119–122	120–124	[51]
4	4-aminophenol	25	90	150	360	186–189	185–189	[51]
5	4-amino-2-chlorophenol	40	90	150	226	150–152	151.5	[51]
6	3-Aminoacetophenone	30	94	157	314	96–98	97	[51]
7	4-Aminoacetophenone	25	99	165	397	105–107	106	[51]
8	Benzene-1,4-diamine	40	96	160	241	139–142	140	[51]
9	3-chloroaniline	30	96	160	320	94-96[b]	95-96[b]	[51]
10	3,4-dichloroaniline	50	92	154	185	70–72	69–71	[51]
11	4-Chloro-1,2-diaminobenzene	35	97	162	278	68–70	68.5	[51]
12	4-bromoaniline	40	81	135	203	66–66.5	66	[51]
13	3-Bromo-4-methoxyaniline	60	70	117	117	61–62	62	[52]
14	2-Aminopyridine	35	90	150	258	57–59	58	[51]
15	2-Aminothiophenol	40	87	145	218	17–21	19	[51]
16	3,4-dimethylbenzene-1,2-diamine	50	72	120	144	87–89	86–90	[53]
17	4-methoxy-2,3-dimethylaniline	60	92	154	154	269[b]	265.4 ± 35[b]	[54]
18	2-aminobenzoic acid	15	86	86	344	142–145	144–148	[51]
19	3-aminobenzoic acid	25	90	90	216	178–180	178–180	[51]
20	4-aminobenzoic acid	20	89	89	267	186–188	189	[51]

[a]Optimised reaction conditions: Nitrobenzene (1 mmol), $NaBH_4$ (3 mmol), and Fe_3O_4@Guanidine-Cu^{II} (0.6 mol%) catalyst were stirred in ambient conditions for 15–60 min. [b]Liquid

Table 3 Emulation of catalytic efficiency of Fe_3O_4@Guanidine-Cu^{II} with previously reported catalysts for reducing nitroarenes

Catalyst (mol%)	Reaction Parameters	Time (h)	Yield (%)	[Ref]
CuNPs (0.003)	$HCOONH_4$, Ethylene glycol, 120 °C	11	86	[55]
CuNPs/WS-1(2)	$NaBH_4$, H_2O, 35 °C	3	93	[56]
Pd-GO/CNT–Fe_3O_4 (1)	H_2, H_2O, 60 °C	3	90	[57]
Cu NPs (10)	$NaBH_4$, THF: H_2O, 50 °C	2	98	[58]
PdCu/graphene (2)	$NaBH_4$, EtOH: H_2O, 50 °C	1.5	96	[59]
Fe_3O_4@Cu (2)	$NaBH_4$, EtOH: H_2O, 50 °C	1.5	95	[60]
$NiFe_2O_4$@Cu (150 mg)	$NaBH_4$, EtOH: H_2O, Reflux	1	95	[61]
Fe_3O_4@C-Pd (40 mg)	$NaBH_4$, EtOH, 25 °C	1	99	[62]
$CuFe_2O_4$ (20)	$NaBH_4$, H_2O, Reflux	0.833	95	[63]
Fe_3O_4@Guanidine-Cu^{II} (0. 6)	$NaBH_4$, EtOH, rt	0.5	99	Present study

Previously reported catalysts had encountered various disadvantages like temperature rise, hazardous organic solvents or reagents usages, non-renewable catalysts involvement, a high amount of catalysts, and combustible hydrogen gas requirements. The synthesized Fe_3O_4@Guanidine-Cu^{II} acted as an effective catalyst in ambient conditions by the existence of $NaBH_4$ in ethanol media, less amount of catalyst (0.6 mol %), magnetically recoverable in good yield, reusable without similar catalytic effect up to eight cycles, and without using any additives. Moreover, Fe_3O_4@Guanidine-Cu^{II} is an effective catalyst for reducing nitro groups due to their convenient procedure and low price.

Reusability study

The essential practical benefits of using heterogeneous catalysts are the catalysts' effortless restoration and the provision for concurrent usages in a subsequent reaction. To check this in the mixture, an external magnet was used to retrieve the Fe_3O_4@Guanidine-Cu^{II} from the nitroarenes reduction reaction without any significant loss of the catalyst. We have discovered that the aforementioned catalyst exhibited great reusability. The reaction mixture was rinsed using ethanol (3 × 5 ml), following the initial use of the catalyst, and the catalyst could be easily separated by the solution mixture with the application of an external magnet. Consecutively recovered catalyst is charged by fresh substrate, hydrogen source, and solvent, and the further reaction was carried out. We were able to recover the catalyst along with further usage about 8 times without significant loss in catalyst quantity and activity, as shown in Fig. 7. Besides the SEM image (Fig. 8) and FT-IR spectra (Fig. 9) of the catalyst shown after eight cycles, the recycled catalyst had very high stability.

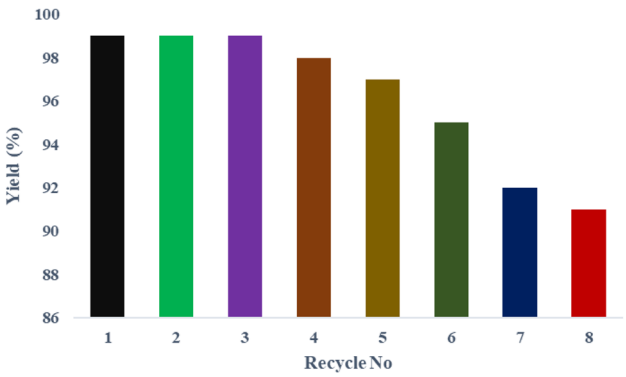

Fig. 8 Reusability of Fe_3O_4@Guanidine-Cu^{II} catalyst in nitroarenes reduction reaction concealed by maximized parameters

Heterogeneity test

Sheldon's test was used to confirm the heterogeneous character of the synthesized material, regardless of any Cu(II) particles were leached in the filtrate solution. The reduction of nitrobenzene was carried out on a nanocatalyst for 15 min under optimal reaction conditions, after which the solution mixture was divided into two halves. The catalyst was removed from one part of the reaction mixture using a magnetic field source and the reaction of both parts was carried out for an additional 15 min. It was found that under non-catalytic environments, no conversion was observed, while the other portion lead to completion as shown in Fig. 10. This also suggests that virtually no leaching of Cu(II) occurred in the reaction mixture, (Fig. 11) which confirms its factual heterogeneity.

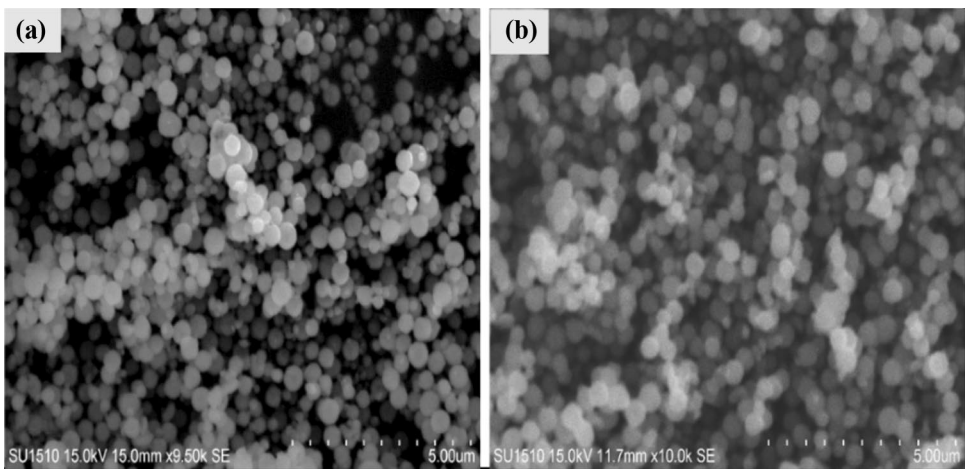

Fig. 9 SEM images of recovered Fe_3O_4@Guanidine-Cu^{II} for **a** before use for catalysis **b** nitroarenes reduction after eight cycles

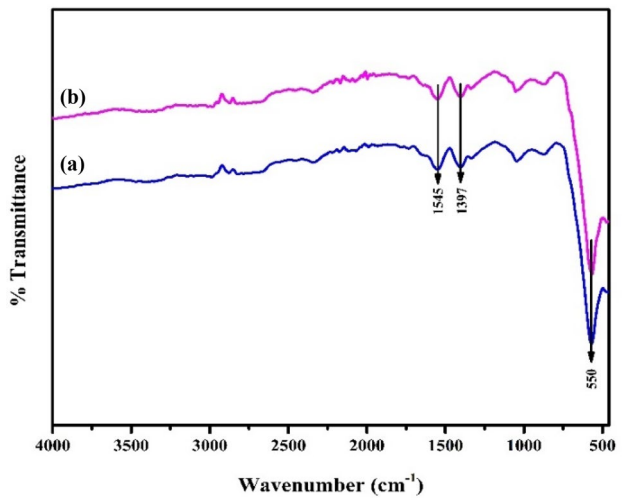

Fig. 10 FTIR spectra of Fe_3O_4@Guanidine-Cu^{II} for **a** before use for catalysis **b** nitroarenes reduction reaction after eight cycles

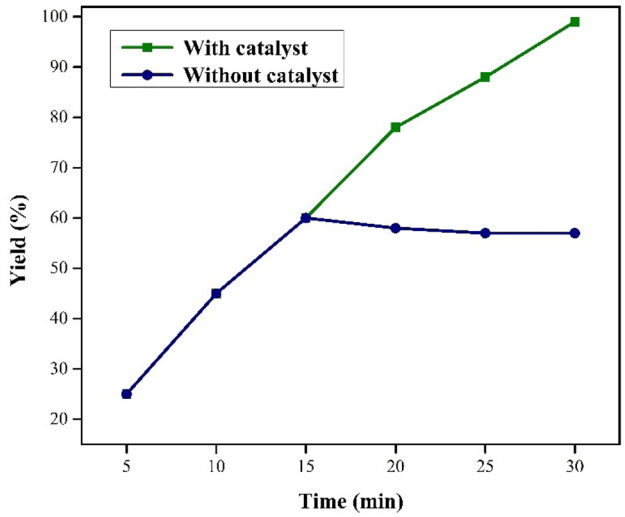

Fig. 11 Hot filtration and leaching test of Fe_3O_4@Guanidine-Cu^{II} in the reduction of nitrobenzene

Plausible mechanism

According to previous reports [49], the plausible mechanism for the reduction of nitroarenes can be proposed, as shown in Scheme 2. At first, the $NaBH_4$ ionizes in presence of liquid surroundings by the formation of borohydride ions $[BH_4]^-$ that is occupied above copper catalyst caused the copper hydride complex (Cu–H) composition. Then, the nitro compounds (C_6H_5–NO_2) are present on the surface of the copper-hydride complex, and both processes are reversible, i.e., adsorption and desorption. If each substrate is chemisorbed on the catalyst surface, hydrogen will

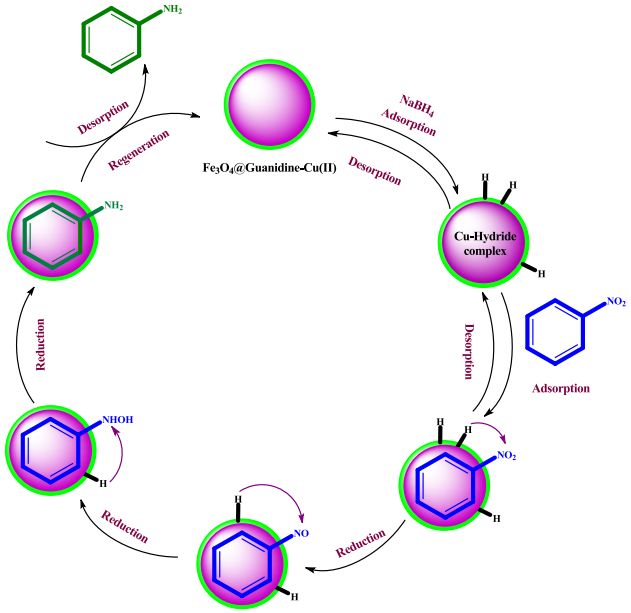

Scheme 2. A plausible mechanism involved in the reduction of nitroarenes

be moved to corresponding amines (C_6H_5–NH_2) from the copper-hydride complex.

Conclusions

This study demonstrated the successful synthesis of Cu^{II} immobilized on guanidine conjugated Fe_3O_4 nanoparticles (Fe_3O_4@Guanidine-Cu^{II}) as an efficient, magnetically recoverable, and reusable heterogeneous catalyst to selectively reduce nitroarenes using $NaBH_4$ as a hydrogen source in ethanol media at ambient conditions. It was observed that Fe_3O_4@Guanidine-Cu^{II} was efficient and could easily reduce substituted nitroarenes to corresponding amines within 25–60 min. The catalyst was easily recovered from the reaction mixture by applying an external magnetic field and also reused for further reaction with excellent yield. The catalyst showed almost unaltered efficacy up to eight cycles of recovery and reuse. Furthermore, all amine derivatives were distinguished by high turnover numbers (TON) and turnover frequency (TOF), demonstrating the increased reaction process as well as refinement of Fe_3O_4@Guanidine-Cu^{II} catalyst in reducing nitroarenes. Applying this kind of effective catalyst for reducing toxic dyes and chemicals can reduce the pollution and cost of producing beneficial compounds also.

Supplementary Information The online version contains supplementary material available at https://doi.org/10.1007/s13738-022-02564-1.

Acknowledgements Authors thank the Department of Science and Technology (DST), Ministry of Science and Technology, Government of India for providing financial assistance by the means of Junior Research Fellowship to Mr. HALLIGUDRA GUDDAPPA concealed by Innovation in Science Pursuit for Inspired Research (INSPIRE) scheme (Sanction No. DST/INSPIRE/03/2015/003933 Registration No: IF160537). KSR are grateful to UGC-BSR faculty fellowship (grant no.F.18-1/2011) (BSR) and DST-PURSE program.

Declarations

Conflict of interest On behalf of all authors, the corresponding author we affirm no conflict of interest.

References

1. J. Tiwari, P. Tarale, S. Sivanesan, A. Bafana, Environ. Sci. Pollut. Res. **26**, 28650 (2019)
2. H. Yang, D. Qi, L. Guo, N. Fan, C. Shao, W. Zhang, L. Yang, Colloid Surface A Physicochem. Eng. Asp. **633**, 127851 (2022)
3. J.B. Sriramoju, C.C. Paramesh, G. Halligudra, D. Rangappa, P.D. Shivaramu, *In photocatalytic syst by des* (Elsevier, London, 2021), pp. 503–536
4. K.H. Liew, T.K. Lee, M.A. Yarmo, K.S. Loh, A.F. Peixoto, C. Freire, R.M. Yusop, Catalysts **9**, 254 (2019)
5. Ö. Bulca, B. Palas, S. Atalay, G. Ersöz, J. Water Process Eng. **40**, 101821 (2021)
6. R. Mudike, C. Sabbanahalli, J.B. Sriramoju, A. Bheemaraju, G. Halligudra, M. Muniyappa, M.P. Narayanaswamy, A. Kumar, P.D. Shivaramu, D. Rangappa, Mater. Res. Bull. **146**, 111606 (2022)
7. K. S. Kiran, R. Shashanka, S. V Lokesh, Top. Catal. (2022).
8. K Kenchappa Somashekharappa, S V Lokesh ACS Omega 6(11): 7248 (2021).
9. S.B. Nair, S.S. Menon, H. Rahman, J.A. Joseph, S. Shaji, R.R. Philip, Semicond. Sci. Technol. **34**, 95023 (2019)
10. C. Chikkanayakanahalli Paramesh, G. Halligudra, V. Gangaraju, J. B. Sriramoju, M. Shastri, H. Kachigere B., P. Habbanakuppe D., D. Rangappa, R. Kanchugarakoppal Subbegowda, and P. Doddakunche Shivaramu, Results in Surfaces and Interfaces 3, 100005 (2021).
11. C.C. Paramesh, G. Halligudra, M. Muniyappa, M. Shetty, K.K. Somashekharappa, D. Rangappa, K.S. Rangappa, P.D. Shivaramu, Ceram. Int. **47**, 14750 (2021)
12. P. Yu, J. Jiang, C. Chen, Z. Wang, D. Wang, G. Li, and X. Li, Catal. Letters 1 (2022).
13. Q. Zhang, J. Guan, Nano Res. **15**, 38 (2022)
14. H. Ding, P. Wang, C. Su, H. Liu, X. Tai, N. Zhang, H. Lv, Y. Lin, W. Chu, X. Wu, C. Wu, Y. Xie, Adv. Mater. **34**(12), 2109188 (2022)
15. H. Geng, Z. Li, D. Li, H. Zhang, X. Wu, L. Zhang, Appl. Catal. A Gen. **631**, 118487 (2022)
16. N. Pradhan, A. Pal, T. Pal, Langmuir **17**, 1800 (2001)
17. M.B. Gawande, A. Goswami, F.-X. Felpin, T. Asefa, X. Huang, R. Silva, X. Zou, R. Zboril, R.S. Varma, Chem. Rev. **116**, 3722 (2016)
18. L. Wang, J. Jiang, J. Ma, S. Pang, T. Zhang, Chem. Eng. J. **427**, 131721 (2022)
19. H. Yu, W. Tang, K. Li, H. Yin, S. Zhao, S. Zhou, Chem. Eng. Sci. **196**, 402 (2019)
20. U. Sharma, P. Kumar, N. Kumar, V. Kumar, B. Singh, Adv. Synth. Catal. **352**, 1834 (2010)
21. R. Jahanshahi, B. Akhlaghinia, New J. Chem. **41**, 7203 (2017)
22. X. Li, D. Liu, S. Song, H. Zhang, Cryst. Growth Des. **14**, 5506 (2014)
23. K. Hasan, I.A. Shehadi, N.D. Al-Bab, A. Elgamouz, Catalysts **9**, 839 (2019)
24. P.D. Shivaramu, A. Patil, M. Murthy, S. Tubaki, M. Shastri, S. Manjunath, V. Gangaraju, D. Rangappa, Mater. Today Proc. **4**, 12314 (2017)
25. R. Jahanshahi, B. Akhlaghinia, Catal. Letters **147**, 2640 (2017)
26. C.W. Jones, Top Catal **53**, 942 (2010)
27. M.S. Ahmed, H. Begum, Y. Kim, J. Power Sour. **451**, 227733 (2020)
28. M. Trivedi, G. Singh, R. Nagarajan, N.P. Rath, Inorganica Chim. Acta **394**, 107 (2013)
29. A. Naghipour, A. Fakhri, Catal. Commun. **73**, 39 (2016)
30. H. Veisi, M. Hamelian, S. Hemmati, J. Mol. Catal. A. Chem. **395**, 25 (2014)
31. A.M. Hollas, W. Gu, N. Bhuvanesh, O.V. Ozerov, Inorg. Chem **50**, 3673 (2011)
32. V.K.R. Kumar, K.R. Gopidas, Tetrahedron Lett. **52**, 3102 (2011)
33. S. Sobhani and Z. Pakdin-parizi, Appl. Catal. A, Gen. 479, 112 (2014)
34. X. Feng, M. Yan, T. Zhang, Y. Liu, M. Bao, Green Chem **12**, 1758 (2010)
35. M. Degardin, S. Wein, J. Duckert, M. Maynadier, A. Guy, T. Durand, R. Escale, H. Vial, Y. Vo-Hoang, ChemMedChem **9**, 300 (2014)
36. B. Atashkar, A. Rostami, B. Tahmasbi, Catal. Sci. Technol. **3**, 2140 (2013)
37. J. Jo, C. Chen, D. Lee, J. Am. Chem. Soc. **135**, 3620–3632 (2013)
38. G. Halligudra, C.C. Paramesh, R. Mudike, M. Ningegowda, D. Rangappa, P.D. Shivaramu, ACS Omega **6**, 34416 (2021)
39. S. Luo, X. Zheng, H. Xu, X. Mi, L. Zhang, J. Cheng, Adv. Synth. Catal. **349**, 2431 (2007)
40. J. Adhikary, A. Datta, S. Dasgupta, A. Chakraborty, M.I. Menendez, T. Chattopadhyay, RSC Adv. **5**, 92634 (2015)
41. F.D. Firuzabadi, Z. Asadi, F. Panahi, RSC Adv. **6**, 101061 (2016)
42. J. Wang, J. Yang, X. Li, B. Wei, D. Wang, H. Song, H. Zhai, X. Li, J. Mol. Catal. A Chem. **406**, 97 (2015)
43. M. Nasrollahzadeh, M. Sajjadi, H.A. Khonakdar, J. Mol. Struct. **1161**, 453 (2018)
44. A. Rostami, B. Atashkar, D. Moradi, Appl. Catal. A Gen. **467**, 7 (2013)
45. E.C.S. Santos, T.C. dos Santos, R.B. Guimarães, L. Ishida, R.S. Freitas, C.M. Ronconi, RSC Adv. **5**, 48031 (2015)
46. A.P. Grosvenor, B.A. Kobe, M.C. Biesinger, N.S. Mcintyre, Surf. Interface Anal. **36**, 1564 (2004)
47. Y. Wang, H. Zhao, M. Li, J. Fan, G. Zhao, Appl. Catal. B Environ. **147**, 534 (2014)
48. C. Bao, H. Zhang, L. Zhou, Y. Shao, J. Ma, Q. Wu, RSC Adv. **5**, 72423 (2015)
49. R.K. Sharma, Y. Monga, A. Puri, J. Mol. Catal. A Chem. **393**, 84 (2014)
50. S. Sobhani, F.O. Chahkamali, J.M. Sansano, RSC Adv. **9**, 1362 (2019)
51. J.-C. Bradley, A. Williams, A. Lang (2014). Dataset (A) https://doi.org/10.6084/m9.figshare.1031638.v1 (B) https://doi.org/10.6084/m9.figshare.1031637.v2
52. T.A. Emokpae, O. Eguavoen, J. Hirst, J. Chem. Soc. Perkin Trans. **2**, 832 (1980)
53. K. Mori, M. Kidawara, M. Iseki, C. Umegaki, T. Kishi, Chem. Pharm. Bull. **46**, 1474 (1998)
54. M. Sako, K. Ichinose, S. Takizawa, H. Sasai, Chem. Asian J. **12**, 1305 (2017)
55. A. Saha, B. Ranu, J. Org. Chem. **73**(17), 6867 (2008)
56. A. Zamani, A. Poursattar Marjani, A. Nikoo, M. Heidarpour, A. Dehghan, Inorg Nano-Metal Chem. 48(11), 176 (2018).

57. F. Yang, A. Feng, C. Wang, S. Dong, C. Chi, X. Jia, L. Zhang, Y. Li, RSC Adv. **6**, 16911 (2016)
58. Z. Duan, G. Ma, W. Zhang, Bull. Korean Chem. Soc. **33**, 10 (2012)
59. Y. Feng, J. Ma, Y. Kang, H. Xu, Tetrahedron **70**, 6100 (2014)
60. S.M. Sajadi, M. Nasrollahzadeh, M. Maham, J. Colloid Interface Sci. **469**, 93 (2016)
61. B. Zeynizadeh, I. Mohammadzadeh, Z. Shokri, S.A. Hosseini, J. Colloid Interface Sci. **500**, 285 (2017)
62. N. Mei, B. Liu, Int. J. Hydrogen Energy **41**, 17960 (2016)
63. B. Zeynizadeh, F.M. Aminzadeh, H. Mousavi, Res. Chem. Intermed. **45**, 3329 (2019)